

A bright burst from FRB 20200120E in a globular cluster of the nearby galaxy M81

S. B. Zhang^{1*}, J. S. Wang^{2*}, X. Yang^{1,3*}, Y. Li¹, J. J. Geng¹, Z. F. Tang^{1,3}, C.M. Chang^{1,3}, J. T. Luo^{4,5}, X. C. Wang⁴, X. F. Wu^{1,3†}, Z. G. Dai^{6‡}, B. Zhang^{7,8§}

¹*Purple Mountain Observatory, Chinese Academy of Sciences, Nanjing 210023, China*

²*Max-Planck-Institut für Kernphysik, Saupfercheckweg 1, D-69117 Heidelberg, Germany*

³*School of Astronomy and Space Sciences, University of Science and Technology of China, Hefei 230026, China*

⁴*National Time Service Center, Chinese Academy of Sciences, Xi'an 710600, China*

⁵*University of Chinese Academy of Sciences, No.19A Yuquan Road, Shijingshan District, Beijing 100049, China*

⁶*Department of Astronomy, University of Science and Technology of China, Hefei 230026, China*

⁷*Nevada Center for Astrophysics, University of Nevada, Las Vegas, NV 89154, USA*

⁸*Department of Physics and Astronomy, University of Nevada, Las Vegas, NV 89154, USA*

Fast radio bursts (FRBs) are immensely energetic millisecond-duration radio pulses. Observations indicate that nearby FRBs can be produced by old stellar populations, as suggested by the localization of the repeating source FRB 20200120E in a globular cluster of M81. Nevertheless, the burst energies of FRB 20200120E are significantly smaller than those of other cosmological FRBs, even falling below the energy of the Galactic event FRB 20200428. Here, we report the detection of a bright burst from FRB 20200120E in 1.1 – 1.7 GHz, with a fluence of ~ 30 Jy ms, which is more than 42 times larger than the previously detected bursts near 1.4 GHz frequency. It reaches one-third of the energy of the weakest burst from FRB 20121102A and is detectable at a distance exceeding 200 Mpc. Our finding bridges the gap between nearby and cosmological FRBs and indicates that FRBs hosted in globular clusters can be bright enough to be observable at cosmological distances.

*These authors contributed equally to this work.

†Email: xfwu@pmo.ac.cn

‡Email: daizg@ustc.edu.cn

§Email: zhang@physics.unlv.edu

Introduction

There are two apparent types of cosmological fast radio bursts (FRBs): repeaters¹ and apparently one-off bursts² (which could be in principle repeaters as well). On the other hand, two nearby events offer clues to the engine and formation channels of FRBs: The apparently one-off burst FRB 20200428 from the Galactic magnetar SGR 1935+2154^{3,4}, points toward a magnetar engine formed from core-collapse supernovae. The FRB 20200120E, identified as a repeating FRB source through the Canadian Hydrogen Intensity Mapping Experiment FRB project (CHIME/FRB)⁵, and then localized by the European Very Long Baseline Interferometry Network (EVN) to a globular cluster [PR95] 30244 in the M81 galactic system at a distance of 3.63 Mpc⁶, points toward an unknown engine formed from a certain delayed channel. It is tempting to generalize these two channels to cosmological FRBs.

High time resolution analysis of the super-narrow components ($\lesssim 100$ ns) of the bursts from FRB 20200120E shows high spectral luminosity^{7,8}, which falls on the low-end of the luminosity distribution of cosmological FRBs. However, considering the burst energy release, there is still a gap between these nearby sources and their cosmological brethren. FRB 20200428^{3,4} was about 1–2 orders of magnitude less energetic than the weakest known extragalactic FRB^{9–11}. Many bursts were detected from FRB 20200120E: CHIME detected three bursts with fluences from 2.0 to 2.4 Jy ms in the frequency band of 400–800 MHz⁵, Effelsberg recorded 65 bursts with fluences from 0.04 to 0.71 Jy ms within the frequency band of 1200–1600 MHz^{6,12}, and DSS-63 observed a burst with a fluence of 0.75 ± 0.15 Jy ms within the frequency band of 2192.5–2307.5 MHz⁷. Nonetheless, FRB 20200120E has even smaller energies, with the most intense burst still less energetic than FRB 20200428. As shown in Figure 3, all previously detected bursts from FRB 20200120E fall roughly in the middle between the Crab super-giant pulses¹³ and typical repeating FRBs^{10,11,14}. One may speculate that the globular cluster channel may not form cosmological FRBs, and hence, cannot be a contributor to the cosmological FRB population.

In this work, we presented the detection of a bright radio burst from FRB 20200120E using the 40-meter Haoping radio telescope. The detection of this bright burst bridges the energy gap between nearby and cosmological FRBs. It suggests that FRBs hosted in globular clusters are bright enough to be observed at cosmological distances, providing further evidence that globular clusters could host cosmological FRBs, at least for the faint population.

Results

In a total of 62.5 hours, we detected a burst within the Epoch 1 data (Methods), which occurred on September 16, 2021, with a barycentric arrival time of 14:39:27.2016 Universal Time (UT) at an infinite frequency. The burst was identified by both PRESTO and HEIMDALL, with a signal-to-noise ratio (S/N) of 13.8 and 11.0, respectively, for the full-band data (1100–1700 MHz). In addition, the narrow-band data (1100–1250 MHz) yielded S/N of 29.8 and 28.3 by PRESTO and HEIMDALL, respectively. Figure 1 presents the dynamic spectra and pulse profile of the detected burst, after being de-dispersed using the optimal DM value of 87.82 pc cm^{-3} (Methods), in general

agreement with previous detections^{5, 7, 12, 15, 16}.

Comparison of the burst with other bursts from FRB 20200120E

The burst has a frequency extent of 1130(4)–1220(4) MHz, a peak flux density of 188 ± 38 Jy, and an averaged fluence of 30 ± 6 Jy ms (see Table 1). This fluence value is ~ 13 times greater than the brightest burst previously detected. Focusing on the L-band, its fluence is 42–754 times brighter than previous ones. An energy distribution analysis of the burst sample from the Effelsberg telescope revealed a steep power-law function with an index of ~ -2.4 at high fluences, and suggest that unless FRB 20200120E has a bi-modal and/or time-variable energy distribution, observations in L-band would be unlikely to detect bursts much exceeding a fluence of 2 Jy ms, such as the detection we made¹². Our only detection with $S/N \sim 30$ and the search threshold of $S/N = 7$ imply a much shallower energy distribution function. This discrepancy might be explained by introducing two distinct energy distributions in different emission states.

As a significant number of bursts within the Effelsberg sample were obtained during a 40-minute burst storm, we divided this Effelsberg dataset into two subsets: bursts in the burst storm and bursts excluding the burst storm. Remarkably, the latter subset displays a relatively flat energy function with the power-law index ~ -0.98 . The detected Haoping burst nicely aligns with the extrapolation of this energy function (Figure 2). Despite being detected at different frequency ranges, it is noteworthy that the bursts recorded by the CHIME and DSS-63 telescopes also align well with the second flatter power-law line. Notably, while the first steep power-law line could also provide a fit for these two samples, our detection significantly deviates from its extrapolation. Incidentally, a two-component energy function has been identified from other active repeating sources¹⁰, with FRB 20201124A showing a flatter power-law tail at higher fluences¹⁷. This suggests that the two-component energy function may be a characteristic of some repeating FRBs.

Based on Equation 1, high luminosities derived from the super-narrow components typically do not significantly increase the detectability of the bursts (Methods). For previous bursts detected at L-band with the largest fluence⁸ and peak flux⁸, the Five-hundred-meter Aperture Spherical Radio Telescope (FAST)¹⁸ could obtain 7σ detections at distances of approximate 43 Mpc and 46 Mpc, respectively. Notably, if positioning FRB 20200120E at a cosmological distance, such as the distance of the nearest localized cosmological repeating FRB 20180916B at 149 Mpc¹⁴, only this bright “Haoping burst” would be detectable by FAST (Methods). Consequently, the repeating FRB 20200120E would appear as a cosmological apparent one-off FRB.

Comparison of the FRB 20200120E with other radio sources

Using the distance to the M81 globular cluster [PR95] 30244 of 3.63 Mpc⁶, we derive a specific luminosity of $3.0 \pm 0.6 \times 10^{30}$ erg s⁻¹ Hz⁻¹ and an isotropic-equivalent energy of $5.6 \pm 1.1 \times 10^{35}$ erg for the burst. This energy is about five times greater than the brightest radio burst from SGR

1935+2154^{3,19}, and is about 1/3 of the weakest burst of FRB 20121102A¹⁰ (Methods). With the inclusion of this newly detected burst, the energy level of FRB 20200120E aligns closely with the main FRB population (Figure 3). The energy release range of this source now spans up to three orders of magnitude.

Discussion

There is compelling evidence that at least some active repeating FRBs track star formation history and therefore originate from prompt formation channels of the FRB engine (such as magnetars)^{20,21}. However, it is still under debate whether all FRBs formed from the prompt formation channels. For instance, analyses of the DM distribution of all FRBs in the first CHIME FRB catalogue^{22,23} indicate the necessity of a delayed population with respect to star formation history together with the prompt population tracking star formation. A subset of the first CHIME FRB catalogue, which excludes bursts of low DM or low DM excess with respect to the Galactic contribution, seems to track star formation history²⁴, similar to some nearby localized FRBs²⁵. The detection of this bright event from FRB 20200120E, which is bright enough to be detected at cosmological distances, suggests that the delayed channel can contribute to the FRB population, at least to the population of faint FRBs. Moreover, few localized FRBs at larger distances have similar or even larger offsets from the centre of the host galaxy than FRB 20200120E (Figure 4). These bursts could be candidates that reside in globular clusters.

The central engine that powers FRB 20200120E remains unclear. Theoretically, there are three possibilities for FRBs in globular clusters (see Methods for details): young magnetar bursts^{26–29}, giant pulses from young pulsars³⁰, and interacting neutron stars^{31–36}. The first two models involve young magnetars or pulsars. In globular clusters, this would require a different formation channel from the core-collapse scenario. It has been suggested that the mergers of compact binary stars, such as white dwarfs and neutron stars, and the accretion-induced collapse of white dwarfs could be potential formation channels^{6,16,37,38}. The interacting neutron stars model involves the release of gravitational energy during the inspiral of a neutron star binary or the collision between asteroids and a neutron star.

However, to date, only one FRB source has been reported to be hosted by a globular cluster, and only one detected burst from this source could be observed at a cosmological distance. The absence of such bursts could be attributed to several factors: (1) The low event rate of bright bursts from these sources. Even with a 1σ confidence level, ~ 360 hours of observation is necessary to detect a burst similar to the “Haoping burst”. (2) The requirement for very sensitive telescopes, which typically have a small field of view (FOV), to detect such bursts at cosmological distances. (3) The current most efficient FRB hunter, CHIME, is only sensitive to such bursts at a distance of $\lesssim 10$ Mpc (Methods), limiting the number of potential host galaxies for generating this phenomenon. Next-generation telescopes that combine both a large FOV and high sensitivity (e.g., SKA) could provide a more complete FRB sample. Until then, searching for more bright bursts from FRB 20200120E with sufficient but not very sensitive observations, and localizing more FRBs in nearby galaxies or globular clusters through specified designed observa-

tional campaigns³⁹, would be valuable for further understanding FRB engines and their formation channels.

Methods

Observations and burst detection

Observations for this study were carried out using the 40 m–diameter Haoping radio telescope, which consists of two epochs: Epoch 1 from September 16 to 17, 2021, lasting 22.7 hours, and Epoch 2 from April 13 to 15, 2023, spanning 39.8 hours. The receiver was within the L-band, covering a frequency range of 1100 to 1700 MHz. The single-polarization signals were 8-bit sampled and channelized using the Reconfigurable Open Architecture Computing Hardware generation 2 (ROACH 2)⁴⁰. Subsequently, the data were stored in the PSRFITS search mode format⁴¹. The specific sample time and channel width for Epoch 1’s observation were set at $40.96 \mu\text{s}$ and 0.195 MHz, respectively. Due to the site’s observation constraints during Epoch 2, the sample time was $81.92 \mu\text{s}$, and the channel width was 0.390 MHz. To verify the observation setup and search pipelines, a bright pulsar PSR J0332+5434 has been observed prior to each FRB 20200120E observation.

The data collected from the Haoping radio telescope were processed to create three different kinds of band datasets for search: the full-band (1100–1700 MHz), half-band (1100–1400 MHz and 1400–1700 MHz) and narrow-band (1100–1250 MHz, 1250–1400 MHz, 1400–1550 MHz and 1550–1700 MHz). These datasets were analysed via two individual search pipelines, based on the pulsar/FRB single pulse searching packages PRESTO⁴² and HEIMDALL⁴³. The datasets were dedispersed in a range of DM values from 78 to 98 cm^{-3} pc, with a step size of 0.01 cm^{-3} .

Any candidate with an S/N greater than seven was recorded and subject to visual inspection. The DM for any detected burst will be derived by maximizing the S/N of its integrated pulse profile. Within the 62.5 hours of observation, a burst was detected in the data from Epoch 1, occurring on September 16, 2021, with a barycentric arrival time of 14:39:27.2016 Universal Time (UT) at an infinite frequency. Both PRESTO and HEIMDALL successfully identified this burst, yielding S/N of 13.8 and 11.0 for the full-band data (1100–1700 MHz), S/N of 22.5 and 18.8 for the half-band data (1100–1400 MHz), and S/N of 29.8 and 28.3 for the narrow-band data (1100–1250 MHz), respectively.

Estimation of flux, fluence, and energy of the burst

To estimate the burst’s flux densities, we employed two methods:

(1) Radiometer equation approach: The expected root-mean-square (RMS) of the off-pulse data in Jy could be derived using the radiometer equation⁴⁴:

$$\Delta S_{\text{sys}} = \frac{T_{\text{sys}}}{G \sqrt{\Delta \nu N_p t_{\text{obs}}}}, \quad (1)$$

where we ignore the loss factor owing to the 8-bit sampling, $\Delta \nu = 90 \text{ MHz}$ and $t_{\text{obs}} = 40.96 \mu\text{s}$ are the specified frequency range (1130–1220 MHz) and time resolution, and $N_p = 1$ as only the right-handed single-polarization was employed. T_{sys} is the system temperature and G is the telescope antenna gain. Notably, the Haoping telescope is equipped with a room-temperature receiver, and the latest measurements of T_{sys} and G for the telescope at L band is $\sim 120\text{K}$ and 0.26K/Jy , respectively, which are consistent with the previously reported values for Haoping⁴⁵ and another similar 40-m telescope from Kunming, China⁴⁶. By calibrating the data using ΔS_{sys} , we obtained a peak flux of $188 \pm 38 \text{ Jy}$, accounting for a 20% uncertainty in system temperature fluctuation. The fluence was computed by integrating the burst flux above the baseline, while the effective width was determined by dividing the fluence by the burst peak flux.

(2) Comparison to known pulsar: Due to the relatively low sensitivity and severe RFI environment of the Haoping telescope, we only used the bright pulsar PSR J0332+5434 as the comparison. We examined data (MJD 59473) of PSR J0332+5434 prior to Epoch 1 and opted for a 30-minute observation minimally affected by radio interference (RFI). To reduce the scintillation impacts, we also examined the Haoping archive of J0332+5434 and obtained an additional three observations (MJD 58831, 59579, 59588) with sufficient tracking ($\geq 30\text{min}$) and minimal RFI impact. The pulsar data were folded using the DSPSR⁴⁷ and PSRCHIVE⁴⁸ packages, based on its time ephemeris⁴⁹. Utilizing the mean flux density at 1400 MHz and the period of PSR J0332+5434⁵⁰, we scaled the fluence of our burst data to Jy ms units based on the four observations of PSR J0332+5434. This approach resulted in a fluence of $25 \pm 8 \text{ Jy ms}$ (corresponding to peak flux of $154 \pm 52 \text{ Jy}$), accounting for a 30% uncertainty related to the variation of pulsar data.

Notably, the flux estimations attained from both methods exhibit congruence. For the main text, we adopted the value derived from the first approach based on the latest measurement for gain and system temperature for the Haoping telescope. The estimation based on the pulsar could be a useful comparison and reference point.

Detectability of the bursts from FRB 20200120E

If positioning this ‘‘Haoping burst’’ at the distance of the nearest other extragalactic repeating FRB, FRB 20180916B at 149 Mpc, it would exhibit a peak flux of approximately 111 mJy. The FAST telescope has a system temperature of $\sim 20\text{K}$ and a gain of 16K/Jy ¹⁸. Based on Equation 1, taking into account $N_p = 2$ and t_{obs} using the burst width, the sensitivity of this high-sensitive instrument at L-band could yield a 16σ detection. For the ‘‘Haoping burst’’, previous bursts detected at L-band with the largest fluence⁸ and peak flux⁸, if sufficient time resolution is available to identify

the bursts, FAST could obtain 7σ detections at distances of approximate 225 Mpc, 43 Mpc and 46 Mpc, respectively.

Additionally, considering the gain and system temperature for CHIME and the Parkes cryoPAF, which are 1.16 K/Jy and 50 K^{51} , and 0.735 K/Jy and 20 K^{52} , respectively, these two instruments could obtain 7σ detection for “Haoping burst” at distances of approximate 37 Mpc and 47 Mpc, respectively. The CHIME FRBs with baseband data could significantly increase source localizations⁵³, enabling the determination of whether bursts with low DM or low DM excesses with respect to the Galactic contribution are extragalactic sources. However, the current CHIME system would only record the baseband data containing real-time detections with high S/N (usually set between 10 and 12) at a time resolution of ~ 1 ms. Such a system would only be sensitive to a burst similar to the “haoping burst” at distances of $\lesssim 10$ Mpc.

Effective time resolution

The effective time resolution of our observations could be estimated by⁵⁴:

$$w_{\text{eff}} = \sqrt{w_{\text{DM}}^2 + w_{\Delta\text{DM}}^2 + w_{\text{sample}}^2}, \quad (2)$$

where w_{DM} is the dispersion smearing $\sim 73 - 107 \mu\text{s}$ at frequency of 1100 – 1250 MHz with channel width of 0.195 MHz, $w_{\Delta\text{DM}}$ is caused by the dedispersion error which can be ignored for our observation, $w_{\text{sample}} = 40.96 \mu\text{s}$ is the sample time of Epoch 1. Our observation has an effective time resolution of approximately from 83 to 114 μs for frequency from 1100 to 1250 MHz. This resolution is similar to the width of the burst we detected of 161 μs . Due to the effective time resolution limit, we can not explore its possible narrower components, which are well studied by DSS-63⁷ and Effelsberg¹⁶. However, it is notable that even derived from such a large time resolution, the peak flux density of our burst of ~ 188 Jy is slightly smaller than their peak flux derived from time resolutions of < 100 ns.

Bursts of FRB 20200120E from different telescopes

In previous studies, burst detections from FRB 20200120E have been reported by three telescopes. According to the CHIME real-time FRB report, eight candidate bursts from this source were identified within the frequency range of 400–800 MHz, yet the properties of only three of them are available⁵. These three bursts were detected from January 20 to November 29, 2020, corresponding to an expected on-source time of about 41 hours⁵⁵. However, the on-source exposure would increase to about 111 hours if one uses the starting date of the CHIME FRB project on July 25, 2018. To avoid included observation of CHIME with different sensitivity at different stages, we only employed the properties and expected exposure time of these three bursts to estimate the event rate of CHIME detections⁵⁶. The Effelsberg telescope recorded a total of 65 bursts, with fluences ranging from 0.04–0.71 Jy ms within the frequency band of 1200–1600 MHz^{6,12}. The

DSS-63 telescope identified a burst with a fluence of 0.75 ± 0.15 Jy ms within the frequency band of 2192.5–2307.5 MHz⁷.

Luminosities and burst durations for various coherent radio pulses.

To ensure consistency with previous investigations of various coherent radio pulses^{16,57}, we presented diverse coherent radio pulses in a two-dimensional plane in Figure 3. The horizontal axis represents the transient width multiplied by the central observing frequency, while the vertical axis depicts the isotropic-equivalent spectral luminosity. The burst detected in this study was present using the central burst frequency. The primary focus of this study is energy release, we omitted the results from the detailed burst temporal structures and applied the effective width or the width of the pulse at 50% of its peak (W_{50}) of the whole event as the burst duration. For pulsars and RRATs, we presented the average properties of pulses from these sources. However, individual pulses could vary in terms of brightness and duration, typically by approximately 1 order of magnitude, with some deviations even reaching up to 3 orders of magnitude⁵⁸. The luminosities were estimated through peak flux density. It's noteworthy that the luminosities of pulsars were calculated using the mean flux density averaged over the pulsar period (P_0)⁴⁴. Throughout this study, we modified the pulsar luminosities to isotropic-equivalent spectral luminosity by multiplying them by the ratio of P_0 to W_{50} .

Estimation and comparison of isotropic-equivalent energy

Three methods could be used to compare the energies of different radio pulses⁵⁹: (1) the specific isotropic-equivalent energy:

$$E_S = \frac{4\pi D_L^2}{1+z} F, \quad (3)$$

where D_L is the luminosity distance, z is the redshift, and F is the pulse fluence. (2) the isotropic-equivalent energy by scaling E_S by central frequency (E_{cf}), and (3) isotropic-equivalent energy by scaling E_S by burst frequency extent (E_{fe}).

As our primary comparisons involve our burst, FRB 20200428³ and FRB 20121102A¹⁰, in the main text, we used (2) to be consistent with their calculations. The estimated energy of our burst, FRB 20200428 and the weakest burst of FRB 20121102A are $\sim 5.6 \times 10^{35}$, 1.1×10^{35} , and 1.7×10^{36} erg, respectively. Applying (1), the estimated specific energy of these three events are $\sim 4.7 \times 10^{26}$, 8.0×10^{25} , and 1.3×10^{27} erg Hz⁻¹, respectively. Applying (3) the estimated energy of these three events are $\sim 4.2 \times 10^{34}$, 1.5×10^{34} , and 1.4×10^{35} erg, respectively.

Comparison of the FRB 20200120E environment with other FRBs

The environments of transients usually reveal the population of the progenitors. In general, progenitors from young populations reside in the central bright region of the host galaxies, with small offsets from the galaxy centres, while those from old populations are in the outer faint region of the host galaxies and have large offsets^{60,61}. FRB 20200120E is located on the edge of the host galaxy, with a large offset of 20_{-2}^{+3} kpc⁵, consistent with a globular cluster origin.

In order to examine whether other FRBs are consistent with a globular cluster origin, we examine the normalized offsets of them with respect to the host galaxy centres based on the available data^{62,63}. In addition, for FRBs that lack host galaxy radius or offset information, we searched for the host galaxy information with the FRB positions in the SDSS, DESI/Legacy Survey as well as Pan-STARRS catalogue, and estimated the offsets with the FRBs and host galaxy position. For host galaxies detected with Pan-STARRS catalogue only, we fit the r -band with GALFIT¹ to obtain the half-light radii as well as the uncertainty. The results are presented in Extended Data Figure 4, which show that a fraction of cosmological FRBs indeed have a normalized offset similar to or larger than that of FRB 20200120E. In particular, FRB 20190611B and FRB 20190523A have normalized offsets of 5.4 ± 2.7 and 8.3 ± 6.9 , respectively⁶², which are away from the stellar light of the host galaxies. These positions are more likely associated with older population environments such as globular clusters.

Implications for FRB models

The observational properties of FRBs (short duration, high brightness temperature, strong linear polarization, etc) have propelled theories involving compact stars, especially neutron stars, as potential sources⁶⁴. These theories encompass scenarios involving highly magnetized neutron stars or magnetars^{26–29}, young Crab-like pulsars³⁰, or various interacting neutron stars in binary systems^{32,34–36} or with small bodies^{31,33}. The fact that the Haoping burst carries an energy level exceeding FRB 20200428 from SGR 1935+2154 and is comparable with the faintest cosmological FRBs raised the perspective of interpreting all FRBs with a unified magnetar engine. Nonetheless, in terms of energetics, several other scenarios are still allowed besides the magnetar model. In the following, we discuss various models in turn.

1. Young magnetar burst model

For the magnetar models, the energy of the bursts mainly comes from the dissipation of internal magnetic energy. For a typical magnetar with an internal field $B_* = 10^{14} B_{14}$ G and a canonical radius $R_{\text{NS}} = 10^6$ cm, the internal magnetic energy is $E_B = 1.67 \times B_{14}^2 10^{45}$ erg. The average energy dissipation rate is

$$\dot{E}_B = E_B/t_{\text{amb}} = 5.6 \times 10^{32} B_{14}^{3.2} \text{ erg/s}, \quad (4)$$

¹<https://users.obs.carnegiescience.edu/peng/work/galfit/galfit.html>

where the dissipation time due to ambipolar diffusion is $t_{\text{amb}} = 2 \times 10^5 B_{14}^{-1.2} \text{ yr}^{26}$. The average isotropic equivalent luminosity of this event over our observation time is $\bar{L} = 5.79 \times 10^{35} \text{ erg}/62.5 \text{ h} = 2.6 \times 10^{30} \text{ erg/s}^{37,38}$. Assuming a radiation efficiency $f_r = 10^{-5} f_{r,-5}$ of the FRB event³, the magnetar producing FRB 20200120E should have an internal magnetic field $B_{14} \approx 6.7 f_{r,-5}^{-0.31}$ and a corresponding dissipation time $t_{\text{amb}} = 9.4 \times 10^3 f_{r,-5}^{-0.375} \text{ yr}$. This suggests that a young magnetar is enough to power this source.

2. Young pulsar giant pulse model

The giant pulse like model assumes that FRBs are powered by the spin-down of NSs³⁰. For a canonical NS with moment of inertia $I_{\text{NS}} \approx 10^{45} \text{ g cm}^2$, the spin-down luminosity due to magnetic dipole radiation is

$$L_{\text{sd}} = 4.8 \times 10^{42} B_{12}^2 P_{-3}^{-4} (1 + t/\tau_{\text{sd}})^{-2} \text{ erg/s}, \quad (5)$$

where $\tau_{\text{sd}} = 130 P_{-3}^2 B_{12}^{-2} \text{ yr}$ is the spin-down time scale of an NS with surface magnetic field $B = 10^{12} B_{12} \text{ G}$ and initial period $P = 10^{-3} P_{-3} \text{ s}$. It can be seen that for $t < \tau_{\text{sd}}$, the luminosity remains almost constant, otherwise it will decrease as $L_{\text{sd}} \propto t^{-2}$. As this FRB is still active, we mainly consider the case of for $t < \tau_{\text{sd}}$. The peak luminosity of this event is $L_p = 3.6 \times 10^{39} \text{ erg/s}$. Taking a radiation efficiency of giant pulses at $f_r = 10^{-1} f_{r,-1}$ ³⁰, we found that the NS needs to have an initial period $P_{-3} \lesssim 2.3 B_{12}^{1/2} f_{r,-2}^{1/4}$ and a corresponding spin down time of $\tau_{\text{sd}} \lesssim 686 B_{12}^{-1} f_{r,-2}^{1/2} \text{ yr}$. Recycled pulsars in globular clusters can have millisecond periods, but with a weak surface magnetic field ($\lesssim 10^{10} \text{ G}$)⁶⁵. Therefore, recycled pulsars can not power such an event, and a young NS is required. However, the possibility of associating with pulsar wind nebulae has been disfavoured from X-ray observation⁶⁶.

3. Interacting neutron star model

There are in general two types of magnetosphere interaction models that form NS binaries: NS-NS inspiral model^{32,34-36} and NS-asteroid interaction model^{31,33}. For the NS-asteroid interaction model, the NS may have a main-sequence star companion, which hosts an asteroid belt. The NS may interact with the asteroids and produce FRBs. The FRB energy mainly comes from the gravitational potential of the planet, which is

$$E = 1.9 \times 10^{38} m_{18} \text{ erg}, \quad (6)$$

for a planet with mass $m = 10^{18} m_{18} \text{ g}^{33}$. For the observed event with energy $8.70 \times 10^{32} - 5.79 \times 10^{35} \text{ erg}^{16}$, this requires asteroids to be $4.7 \times 10^{12} - 3.1 \times 10^{15} \text{ g}$.

The NS-NS spiral model is usually supposed to be responsible for non-repeating FRBs, as it can produce a luminous event during the last orbits. But it also works when the NSs are widely separated, although the luminosity will become much lower. For two NSs with equal surface magnetic field and anti-parallel magnetic axes, the electromagnetic luminosity from magnetosphere interaction is

$$L_{\text{inspiral}} = 3.4 \times 10^{39} B_{12}^2 a_9^{-2} \text{ erg/s}, \quad (7)$$

at a separation of $a = 10^9 a_9 \text{ cm}$ ³⁴. While the merger time for NSs with mass $M = 1.4M_\odot$ is $t_{\text{merger}} = 3.2a_9^4 \text{ yr}$ for binaries with separation $a \gg R_{\text{NS}}$ assuming a circular orbit. Again assuming the radiation efficiency of giant pulses, the requirement on the surface magnetic field of both NSs is $B_{12} = 3.2a_9 f_{r,-1}^{-1/2}$. Therefore, in principle, NS-NS inspiral cannot be excluded from this event, which could potentially serve as a new type of electromagnetic counterpart of gravitational wave events.

1. Spitler, L. *et al.* A Repeating Fast Radio Burst. *Nature* **531**, 202 (2016). 1603.00581.
2. Lorimer, D. R., Bailes, M., McLaughlin, M. A., Narkevic, D. J. & Crawford, F. A Bright Millisecond Radio Burst of Extragalactic Origin. *Science* **318**, 777 (2007). 0709.4301.
3. Bochenek, C. D. *et al.* A fast radio burst associated with a Galactic magnetar. *Nature* **587**, 59–62 (2020). 2005.10828.
4. CHIME/FRB Collaboration *et al.* A bright millisecond-duration radio burst from a Galactic magnetar. *Nature* **587**, 54–58 (2020). 2005.10324.
5. Bhardwaj, M. *et al.* A Nearby Repeating Fast Radio Burst in the Direction of M81. *ApJ* **910**, L18 (2021). 2103.01295.
6. Kirsten, F. *et al.* A repeating fast radio burst source in a globular cluster. *Nature* **602**, 585–589 (2022). 2105.11445.
7. Majid, W. A. *et al.* A Bright Fast Radio Burst from FRB 20200120E with Sub-100 Nanosecond Structure. *ApJ* **919**, L6 (2021). 2105.10987.
8. Nimmo, K. *et al.* Highly polarized microstructure from the repeating FRB 20180916B. *Nature Astronomy* **5**, 594–603 (2021). 2010.05800.
9. Marcote, B. *et al.* A repeating fast radio burst source localized to a nearby spiral galaxy. *Nature* **577**, 190–194 (2020). 2001.02222.
10. Li, D. *et al.* A bimodal burst energy distribution of a repeating fast radio burst source. *Nature* **598**, 267–271 (2021). 2107.08205.
11. Xu, H. *et al.* A fast radio burst source at a complex magnetized site in a barred galaxy. *Nature* **609**, 685–688 (2022). 2111.11764.
12. Nimmo, K. *et al.* A burst storm from the repeating FRB 20200120E in an M81 globular cluster. *MNRAS* **520**, 2281–2305 (2023). 2206.03759.
13. Bera, A. & Chengalur, J. N. Super-giant pulses from the Crab pulsar: energy distribution and occurrence rate. *MNRAS* **490**, L12–L16 (2019). 1909.13812.
14. Chime/Frb Collaboration *et al.* Periodic activity from a fast radio burst source. *Nature* **582**, 351–355 (2020). 2001.10275.
15. Kirsten, F. *et al.* Detection of two bright radio bursts from magnetar SGR 1935 + 2154. *Nature Astronomy* **5**, 414–422 (2021). 2007.05101.
16. Nimmo, K. *et al.* Burst timescales and luminosities as links between young pulsars and fast radio bursts. *Nature Astronomy* **6**, 393–401 (2022). 2105.11446.
17. Kirsten, F. *et al.* Connecting repeating and non-repeating fast radio bursts via their energy distributions. *arXiv e-prints* arXiv:2306.15505 (2023). 2306.15505.

18. Jiang, P. *et al.* The fundamental performance of FAST with 19-beam receiver at L band. *Research in Astronomy and Astrophysics* **20**, 064 (2020). 2002.01786.
19. Zhou, P. *et al.* Revisiting the Distance, Environment, and Supernova Properties of SNR G57.2+0.8 that Hosts SGR 1935+2154. *ApJ* **905**, 99 (2020). 2005.03517.
20. Fong, W.-f. *et al.* Chronicling the Host Galaxy Properties of the Remarkable Repeating FRB 20201124A. *ApJ* **919**, L23 (2021). 2106.11993.
21. Dong, Y. *et al.* Mapping Obscured Star Formation in the Host Galaxy of FRB 20201124A. *arXiv e-prints* arXiv:2307.06995 (2023). 2307.06995.
22. Zhang, R. C. & Zhang, B. The CHIME Fast Radio Burst Population Does Not Track the Star Formation History of the Universe. *ApJ* **924**, L14 (2022). 2109.07558.
23. Hashimoto, T. *et al.* Energy functions of fast radio bursts derived from the first CHIME/FRB catalogue. *MNRAS* **511**, 1961–1976 (2022). 2201.03574.
24. Shin, K. *et al.* Inferring the Energy and Distance Distributions of Fast Radio Bursts Using the First CHIME/FRB Catalog. *ApJ* **944**, 105 (2023). 2207.14316.
25. Bhardwaj, M. *et al.* Host Galaxies for Four Nearby CHIME/FRB Sources and the Local Universe FRB Host Galaxy Population. *arXiv e-prints* arXiv:2310.10018 (2023). 2310.10018.
26. Beloborodov, A. M. A Flaring Magnetar in FRB 121102? *ApJ* **843**, L26 (2017). 1702.08644.
27. Kumar, P., Lu, W. & Bhattacharya, M. Fast radio burst source properties and curvature radiation model. *MNRAS* **468**, 2726–2739 (2017). 1703.06139.
28. Yang, Y.-P. & Zhang, B. Bunching Coherent Curvature Radiation in Three-dimensional Magnetic Field Geometry: Application to Pulsars and Fast Radio Bursts. *ApJ* **868**, 31 (2018). 1712.02702.
29. Lu, W., Kumar, P. & Zhang, B. A unified picture of Galactic and cosmological fast radio bursts. *MNRAS* **498**, 1397–1405 (2020). 2005.06736.
30. Cordes, J. M. & Wasserman, I. Supergiant pulses from extragalactic neutron stars. *MNRAS* **457**, 232–257 (2016). 1501.00753.
31. Geng, J. J. & Huang, Y. F. Fast Radio Bursts: Collisions between Neutron Stars and Asteroids/Comets. *ApJ* **809**, 24 (2015). 1502.05171.
32. Wang, J.-S., Yang, Y.-P., Wu, X.-F., Dai, Z.-G. & Wang, F.-Y. Fast Radio Bursts from the Inspiral of Double Neutron Stars. *ApJ* **822**, L7 (2016). 1603.02014.

33. Dai, Z. G., Wang, J. S., Wu, X. F. & Huang, Y. F. Repeating Fast Radio Bursts from Highly Magnetized Pulsars Traveling through Asteroid Belts. *ApJ* **829**, 27 (2016). 1603.08207.
34. Wang, J.-S., Peng, F.-K., Wu, K. & Dai, Z.-G. Pre-merger Electromagnetic Counterparts of Binary Compact Stars. *ApJ* **868**, 19 (2018). 1810.00170.
35. Zhang, B. Charged Compact Binary Coalescence Signal and Electromagnetic Counterpart of Plunging Black Hole-Neutron Star Mergers. *ApJ* **873**, L9 (2019). 1901.11177.
36. Zhang, B. Fast Radio Bursts from Interacting Binary Neutron Star Systems. *ApJ* **890**, L24 (2020). 2002.00335.
37. Kremer, K., Piro, A. L. & Li, D. Dynamical Formation Channels for Fast Radio Bursts in Globular Clusters. *ApJ* **917**, L11 (2021). 2107.03394.
38. Lu, W., Beniamini, P. & Kumar, P. Implications of a rapidly varying FRB in a globular cluster of M81. *MNRAS* **510**, 1867–1879 (2022). 2107.04059.
39. Kremer, K., Li, D., Lu, W., Piro, A. L. & Zhang, B. Prospects for Detecting Fast Radio Bursts in the Globular Clusters of Nearby Galaxies. *ApJ* **944**, 6 (2023). 2210.04907.
40. Hickish, J. *et al.* A Decade of Developing Radio-Astronomy Instrumentation using CASPER Open-Source Technology. *Journal of Astronomical Instrumentation* **5**, 1641001–12 (2016). 1611.01826.
41. Hotan, A. W., van Straten, W. & Manchester, R. N. PSRCHIVE and PSRFITS: An Open Approach to Radio Pulsar Data Storage and Analysis. *Publications of the Astronomical Society of Australia* **21**, 302–309 (2004). astro-ph/0404549.
42. Ransom, S. M. *New search techniques for binary pulsars*. Ph.D. thesis, Harvard University, Massachusetts (2001).
43. Petroff, E. *et al.* A real-time fast radio burst: polarization detection and multiwavelength follow-up. *MNRAS* **447**, 246–255 (2015). 1412.0342.
44. Lorimer, D. R. & Kramer, M. *Handbook of Pulsar Astronomy*, vol. 4 (2004).
45. Luo, J.-T. *et al.* Pulsar timing observations with Haoping Radio Telescope. *Research in Astronomy and Astrophysics* **20**, 111 (2020). 2003.08586.
46. Men, Y. P. *et al.* Piggyback search for fast radio bursts using Nanshan 26 m and Kunming 40 m radio telescopes - I. Observing and data analysis systems, discovery of a mysterious peryton. *MNRAS* **488**, 3957–3971 (2019). 1907.13056.
47. van Straten, W. & Bailes, M. DSPSR: Digital Signal Processing Software for Pulsar Astronomy. *Publications of the Astronomical Society of Australia* **28**, 1–14 (2011). 1008.3973.

48. van Straten, W., Demorest, P. & Osłowski, S. Pulsar Data Analysis with PSRCHIVE. *Astronomical Research and Technology* **9**, 237–256 (2012). 1205.6276.
49. Hobbs, G., Lyne, A. G., Kramer, M., Martin, C. E. & Jordan, C. Long-term timing observations of 374 pulsars. *MNRAS* **353**, 1311–1344 (2004).
50. Lorimer, D. R., Yates, J. A., Lyne, A. G. & Gould, D. M. Multifrequency flux density measurements of 280 pulsars. *MNRAS* **273**, 411–421 (1995).
51. CHIME/FRB Collaboration *et al.* Observations of fast radio bursts at frequencies down to 400 megahertz. *Nature* **566**, 230–234 (2019). 1901.04524.
52. Manchester, R. N. *et al.* The Parkes multi-beam pulsar survey - I. Observing and data analysis systems, discovery and timing of 100 pulsars. *MNRAS* **328**, 17–35 (2001). astro-ph/0106522.
53. The CHIME/FRB Collaboration *et al.* Updating the first CHIME/FRB catalog of fast radio bursts with baseband data. *arXiv e-prints* arXiv:2311.00111 (2023). 2311.00111.
54. Cordes, J. M. & McLaughlin, M. A. Searches for Fast Radio Transients. *ApJ* **596**, 1142–1154 (2003). astro-ph/0304364.
55. CHIME/FRB Collaboration *et al.* The First CHIME/FRB Fast Radio Burst Catalog. *ApJS* **257**, 59 (2021). 2106.04352.
56. Gehrels, N. Confidence Limits for Small Numbers of Events in Astrophysical Data. *ApJ* **303**, 336 (1986).
57. Bailes, M. The discovery and scientific potential of fast radio bursts. *Science* **378**, abj3043 (2022). 2211.06048.
58. Zhang, S. B. *et al.* RRAT J1913+1330: an extremely variable and puzzling pulsar. *arXiv e-prints* arXiv:2306.02855 (2023). 2306.02855.
59. Zhang, B. Fast Radio Burst Energetics and Detectability from High Redshifts. *ApJ* **867**, L21 (2018). 1808.05277.
60. Bloom, J. S., Kulkarni, S. R. & Djorgovski, S. G. The Observed Offset Distribution of Gamma-Ray Bursts from Their Host Galaxies: A Robust Clue to the Nature of the Progenitors. *AJ* **123**, 1111–1148 (2002). astro-ph/0010176.
61. Fong, W. & Berger, E. The Locations of Short Gamma-Ray Bursts as Evidence for Compact Object Binary Progenitors. *ApJ* **776**, 18 (2013). 1307.0819.
62. Bhandari, S. *et al.* Characterizing the Fast Radio Burst Host Galaxy Population and its Connection to Transients in the Local and Extragalactic Universe. *AJ* **163**, 69 (2022). 2108.01282.

63. Law, C. J. *et al.* Deep Synoptic Array Science: First FRB and Host Galaxy Catalog. *arXiv e-prints* arXiv:2307.03344 (2023). 2307.03344.
64. Zhang, B. The physics of fast radio bursts. *Reviews of Modern Physics* **95**, 035005 (2023). 2212.03972.
65. Manchester, R. N., Hobbs, G. B., Teoh, A. & Hobbs, M. The Australia Telescope National Facility Pulsar Catalogue. *AJ* **129**, 1993–2006 (2005). astro-ph/0412641.
66. Pearlman, A. B. *et al.* Multiwavelength Constraints on the Origin of a Nearby Repeating Fast Radio Burst Source in a Globular Cluster. *arXiv e-prints* arXiv:2308.10930 (2023). 2308.10930.
67. Kulkarni, S. R. Dispersion measure: Confusion, Constants & Clarity. *arXiv e-prints* arXiv:2007.02886 (2020). 2007.02886.
68. Pleunis, Z. *et al.* LOFAR Detection of 110-188 MHz Emission and Frequency-dependent Activity from FRB 20180916B. *ApJ* **911**, L3 (2021). 2012.08372.
69. Good, D. & Chime/Frb Collaboration. CHIME/FRB Detection of Three More Radio Bursts from SGR 1935+2154. *The Astronomer's Telegram* **14074**, 1 (2020).
70. Zhu, W. *et al.* A radio pulsar phase from SGR J1935+2154 provides clues to the magnetar FRB mechanism. *arXiv e-prints* arXiv:2307.16124 (2023). 2307.16124.

Data availability

RRATALOG (<https://rratalog.github.io/rratalog/>)

Data are available upon request. These data are in a public archive at https://github.com/Astroyx/M81_FRB_haoping

Code availability

PRESTO (<http://www.cv.nrao.edu/~sransom/presto/>)

HEMIDALL (<https://sourceforge.net/projects/heimdall-astro/>)

PSRCHIVE (<http://psrchive.sourceforge.net>)

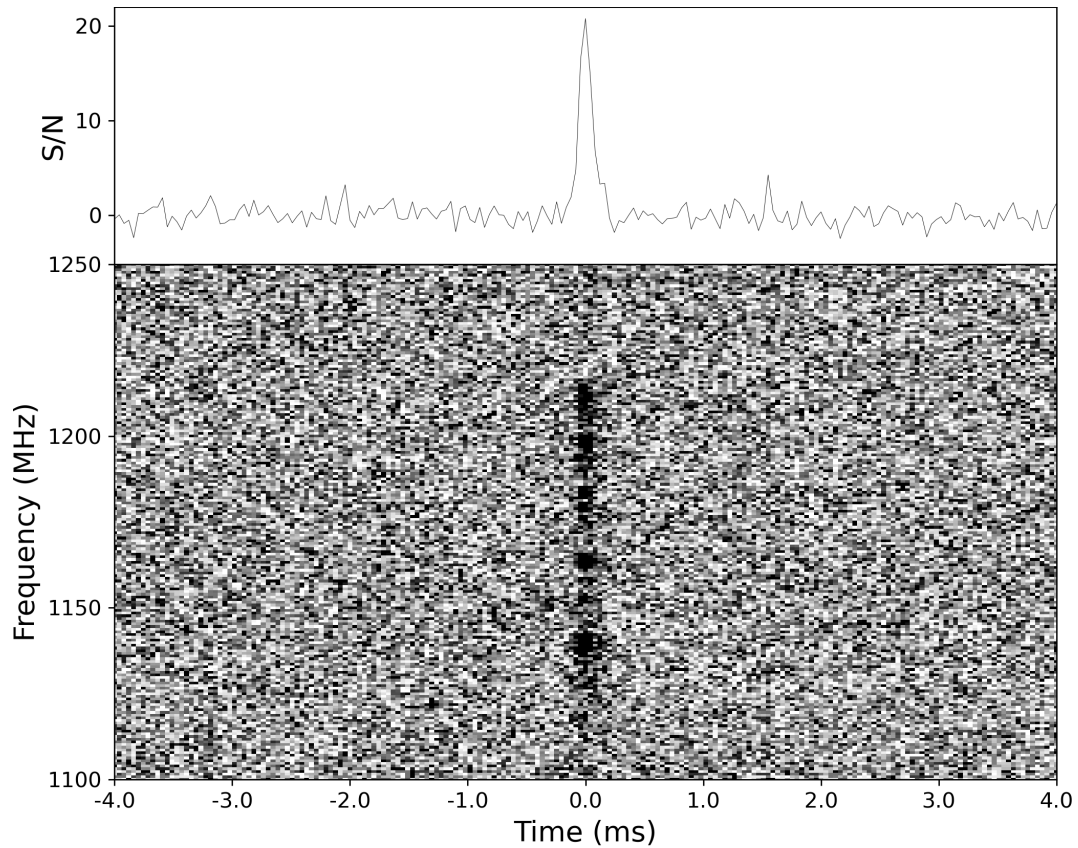


Figure 1: **Integrated pulse profile (top) and dynamic spectra (bottom) of the burst.** The burst is plotted with time and frequency resolutions of $40.96 \mu\text{s}$ and 0.78 MHz , respectively, after being de-dispersed using a DM of 87.82 pc cm^{-3} .

Table 1: **The properties of the bright burst from FRB 20200120E.**

Property	Measurement
Time of arrival ^a (MJD)	59473.6107315
DM (pc cm ⁻³)	87.82(1) ^b
Width ^c (ms)	0.161(3)
Frequency extent ^d (MHz)	1130(4)–1220(4)
Peak flux density (Jy)	188(38)
Fluence (Jy ms)	30(6)
Specific luminosity ^e (erg s ⁻¹ Hz ⁻¹)	3.0(6) × 10 ³⁰
Specific energy release ^e (erg Hz ⁻¹)	4.8(9) × 10 ²⁶
Isotropic-equivalent energy ^f (erg)	5.6(1.1) × 10 ³⁵

^a Corrected to the Solar System Barycentre to infinite frequency, assuming a dispersion measure of 87.82 pc cm⁻³ and using a DM-constant of $a = 4.1488064239^{67}$.

^b Determined by maximizing the S/N of the integrated pulse profile.

^c Effective width.

^d As the signal is close to the low-frequency band edge, we are not sure if the signal exists below 1100 MHz.

^e The specific luminosity/energy release was estimated by scaling the peak flux/fluence by $4\pi D^2$, where D is the distance to [PR95] 30244 .

^f To be consistent with the calculations applied to FRB 20200428³ and FRB 20121102A¹⁰, the isotropic-equivalent energy was estimated by scaling the specific energy release by $\nu_0 = 1175$ MHz, which is the midpoint of the burst frequency range (see Methods for different definitions).

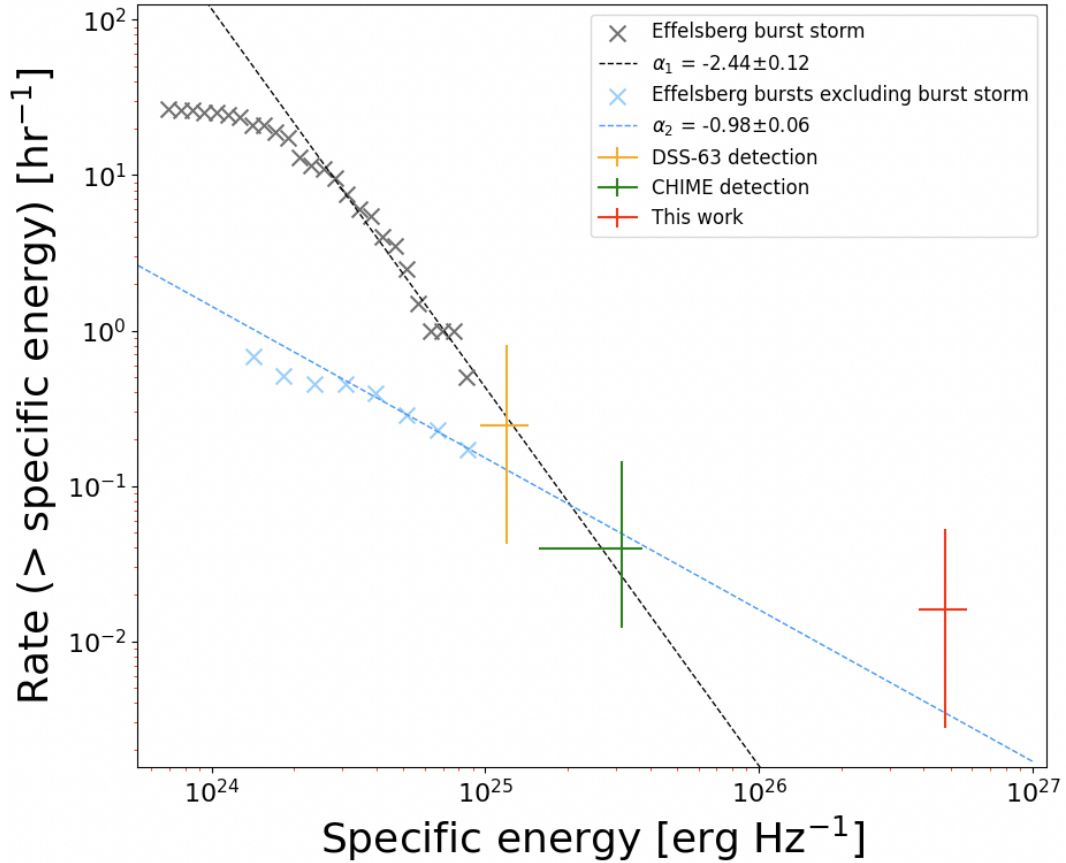


Figure 2: **Distribution of specific energies for bursts originating from FRB 20200120E.** The scatter markers in gray and light blue correspond to the burst storm and other bursts detected by the Effelsberg telescope, respectively. These bursts were fitted with dashed black and blue power law lines for higher fluences, respectively. The orange, green, and red crosses represent bursts with associated errorbars detected by the DSS-63 telescopes, CHIME telescopes, and this work, respectively (see Methods). Notably, the bursts of the CHIME and DSS-63 telescopes were detected at different frequency ranges.

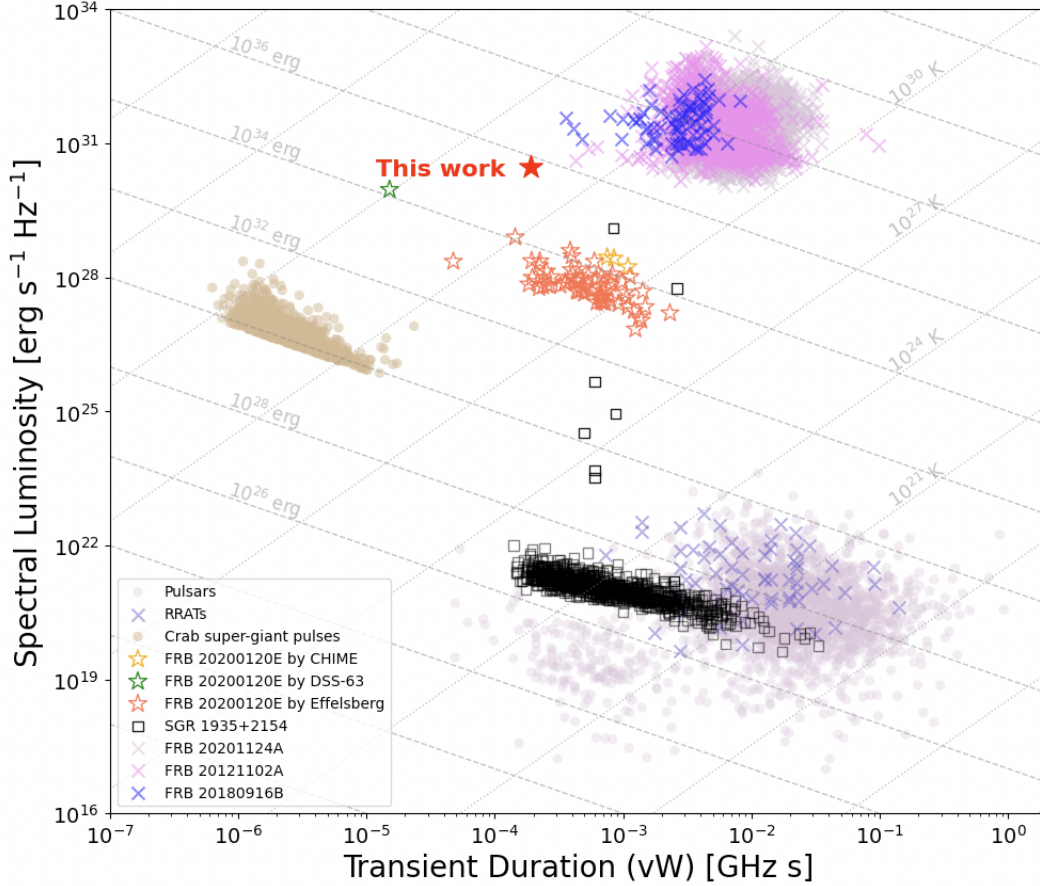


Figure 3: **Isotropic-equivalent spectral luminosity versus the product of observing frequency and pulse width for various coherent radio pulses.** The brightest burst from FRB 20200120E, detected in this study, is denoted by the red-filled star. Other bursts from FRB 20200120E, observed by CHIME⁵, DSS-63⁷, and Effelsberg telescopes^{6,12}, are represented by the orange, green, and tomato unfilled stars, respectively. Three well-studied localized repeating FRBs with known distances are also plotted: FRB 20121102A¹⁰ in violet crosses, FRB 20201124A¹¹ in thistle crosses, and FRB 20180916B^{8,14,68} in blue crosses. Radio bursts or pulses from the Galactic magnetar SGR 1935+2154^{3,4,15,69,70} are denoted by black squares, while super-giant pulses from the Crab pulsar¹³ are shown in tan. The pulsar⁶⁵ and rotating radio transient (RRAT) populations (RRATalog) are marked in thistle and slateblue, respectively. The grey dashed lines denote constant isotropic-equivalent energy release, with no clear gap existing between various radio pulses. The grey dotted lines represent constant brightness temperature.

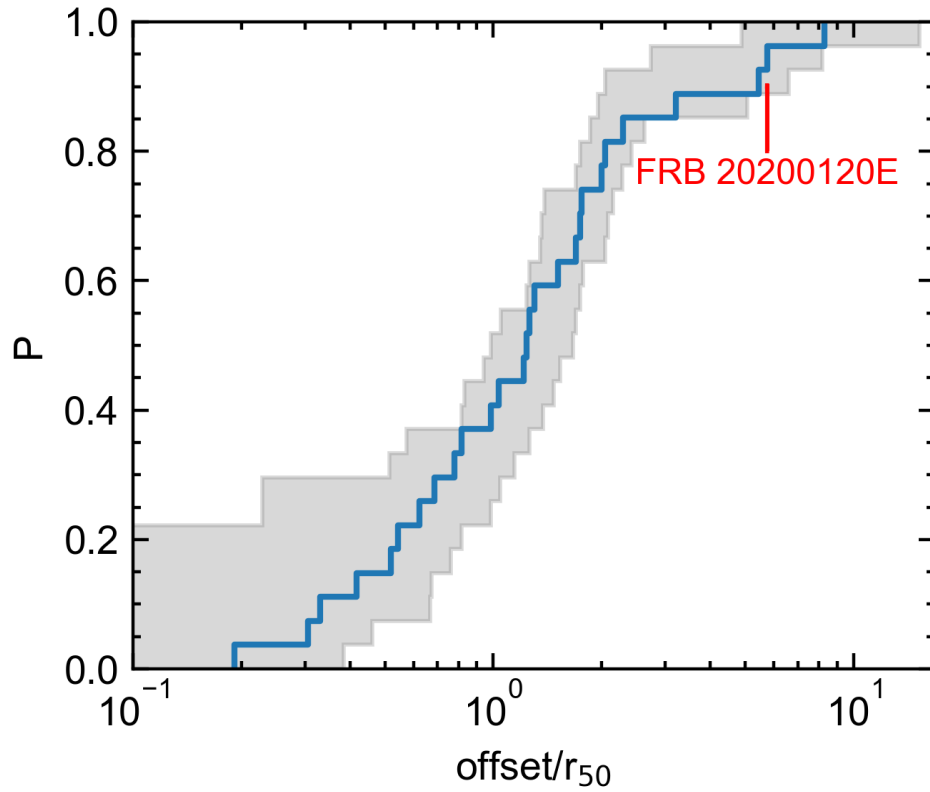


Figure 4: **Cumulative distribution of FRB offsets.** The offset of 27 FRBs from the center of the host galaxies, normalized to the half-light radii r_{50} of the hosts. The blue line and gray region represent median value and 1σ uncertainty. One can see that a few FRBs have normalized offsets comparable to that of FRB 20200120E.

Acknowledgements We thank Apurba Bera for the Crab data. This work is partially supported by the National SKA Program of China (2022SKA0130100,2020SKA0120300), the National Natural Science Foundation of China (grant Nos. 12041306, 12273113,12233002,12003028,12321003), the International Partnership Program of Chinese Academy of Sciences for Grand Challenges (114332KYSB20210018) and the ACAMAR Postdoctoral Fellow. JYG acknowledges the support from the Youth Innovation Promotion Association (2023331). JSW acknowledges the support from the Alexander von Humboldt Foundation.

Author Contributions SBZ, JSW and XFW launched the Haoping observation of FRB 20200120E; SBZ, XY, ZFT, CMC, JTL and XCW carried out the observation and processed the data; BZ, ZGD, JSW, YL and JYG analysed the results and discussed the theoretical models. All authors contributed to the analysis or interpretation of the data and to the final version of the manuscript.

Competing Interests The authors declare that they have no competing financial interests.

Correspondence Correspondence and requests for materials should be addressed to X. F. Wu, Z. G. Dai or B. Zhang.